Supporting Information

Campbell et al. 10.1073/pnas.1413763111

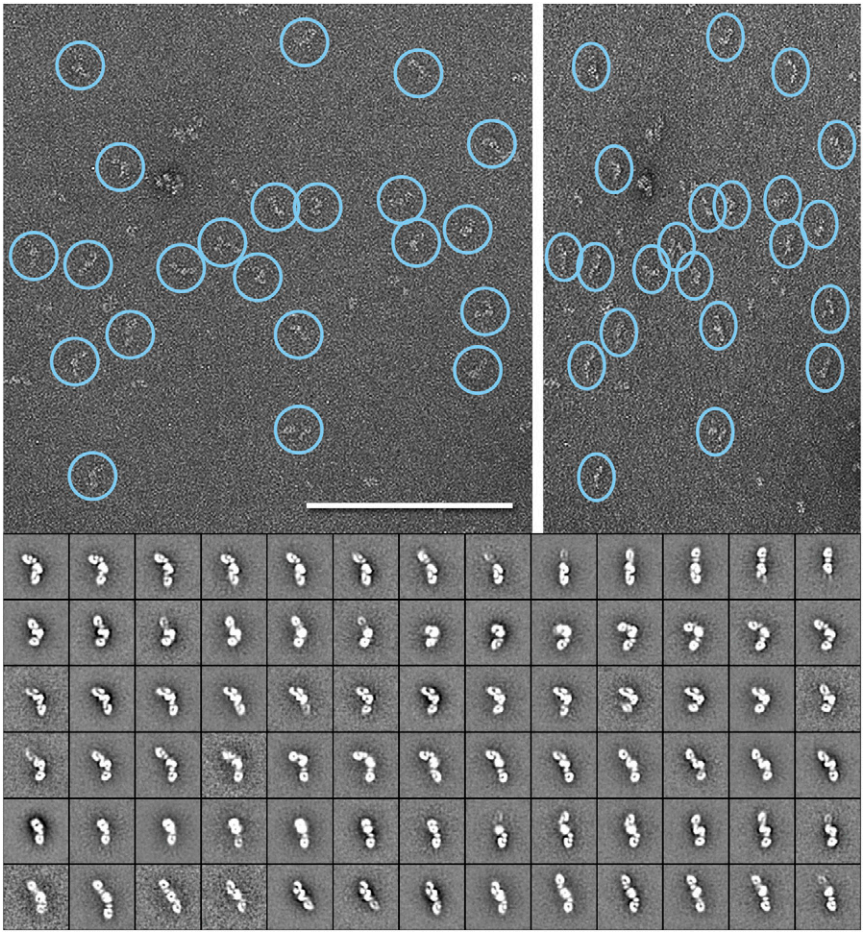

Fig. S1. Inducible NOS (iNOS) data collection and initial processing. (A) iNOS tilt pair of micrographs. Two micrographs of the same area on the grid are shown at 0° tilt (*Left*) and −55° tilt (*Right*). Both micrographs were imaged at a nominal 2-μm underfocus. Exemplary particles used for subsequent alignment and reconstruction are circled in blue. (Scale bar: 200 nm.) (*B*) Reference-based 2D class averages. All 78 class averages were reconstructed into 3D by using the random conical tilt strategy. Only 45 of the maps were consistent with their 2D class averages. The class averages that did not reconstruct well are likely made up of misaligned particles.

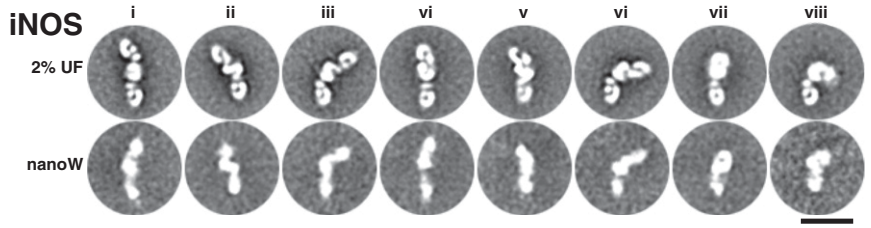

Fig. S2. iNOS conformations are not affected by stain pH. (*Upper*) iNOS stained with 2% uranyl formate (UF) negative stain. (*Lower*) iNOS stained with nanoW neutral pH stain. The loss of detail in the nanoW class averages was anticipated, as uranyl stains have been found to consistently generate the highest contrast of the commonly used stains (1). The higher contrast of uranyl stains facilitates subsequent alignment procedures, which results in higher-resolution images. All 2D class averages comprised 100–350 individual particles. (Scale bar: 20 nm.)

1. Ohi M, Li Y, Cheng Y, Walz T (2004) Negative staining and image classification - powerful tools in modern electron microscopy. *Biol Proced Online* 6:23–34.

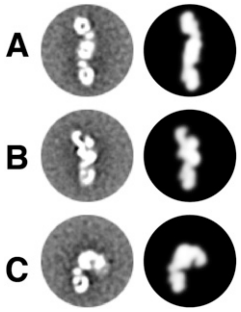

Fig. S3. Comparison of 2D class averages and forward projections of iNOS show consistent structures. The 2D class averages used to produce the 3D reconstructions in Fig. 4 for group I (*A*), group II (*B*), and group III (*C*) are shown in the first column. The models built through fitting crystal structures and homology models of the individual domains, as shown in Fig. 4, were low-pass filtered to 40 Å to produce the forward projections shown in the second column.

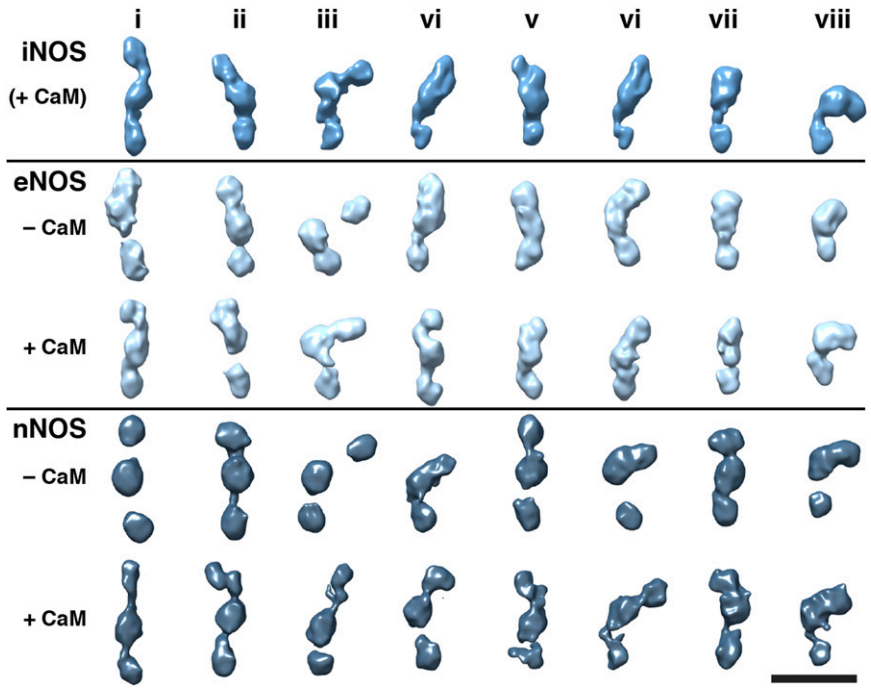

Fig. S4. NOS isoform 3D reconstructions in the presence and absence of calmodulin. These 3D reconstructions correspond to the 2D averages in the same row and column as Fig. 6. (Scale bar: 20 nm.)

Table S1. Steady-state kinetic characterization of iNOS WT and E660R

Mutant	Cytochrome *c* reduction, s^{-1}	DCIP reduction, s^{-1}	Ferricyanide reduction, s^{-1}	NADPH oxidation, s^{-1}	NO formation, s^{-1}
WT	1.50 ± 0.29	1.57 ± 0.14	54.5 ± 5.2	1.08 ± 0.13*	0.48 ± 0.02
iNOS E660R	0.57 ± 0.10	1.70 ± 0.26	54.2 ± 7.9	2.08 ± 0.33	0.60 ± 0.10

Rates were determined as detailed in *Materials and Methods*. Errors represent SD from the mean for at least five independent replicates. DCIP, 2,6-dichlorophenol-indophenol; iNOS, inducible NOS.
*Value from Smith et al. (1).

1. Smith BC, Underbakke ES, Kulp DW, Schief WR, Marletta MA (2013) Nitric oxide synthase domain interfaces regulate electron transfer and calmodulin activation. *Proc Natl Acad Sci USA* 110(38):E3577–E3586.

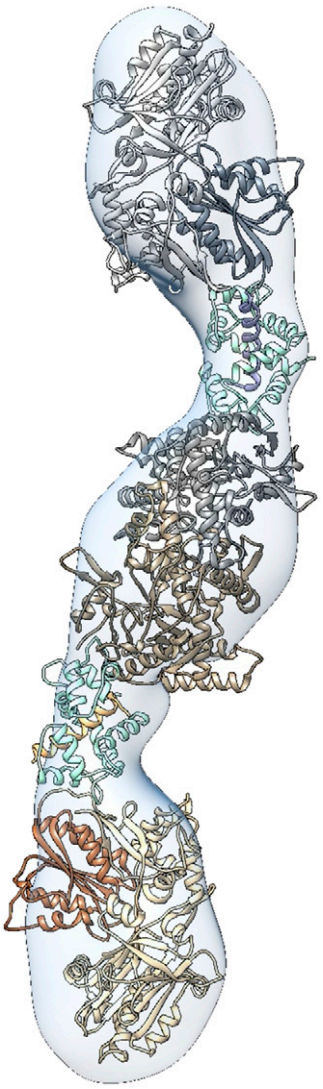

Movie S1. A 360° rotation of a group I (input state) EM structure fit with crystal structures and homology models.

Movie S1

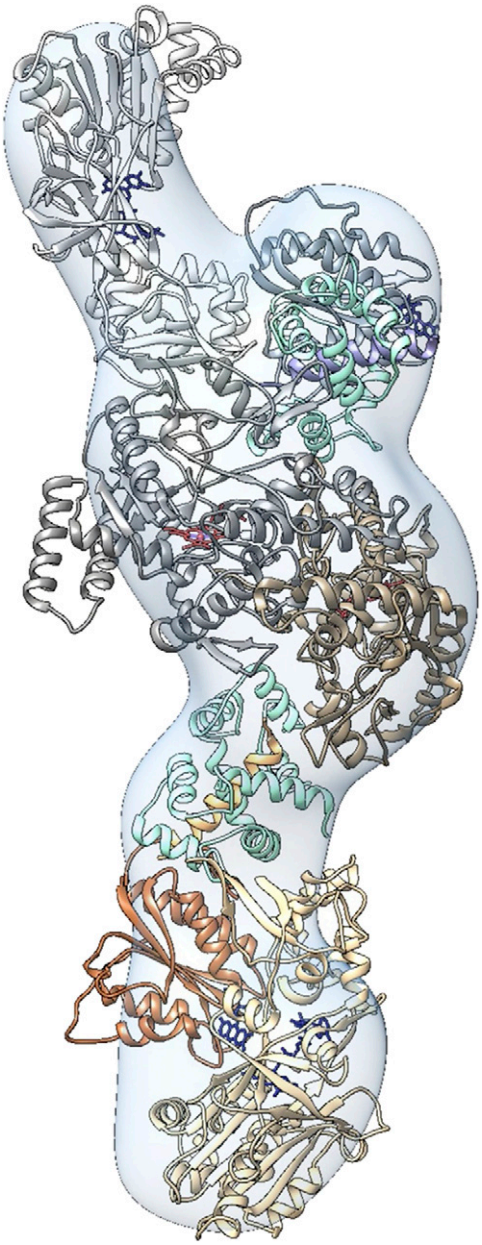

Movie S2. A 360° rotation of a group II (intermediate state) EM structure fit with crystal structures and homology models.

Movie S2

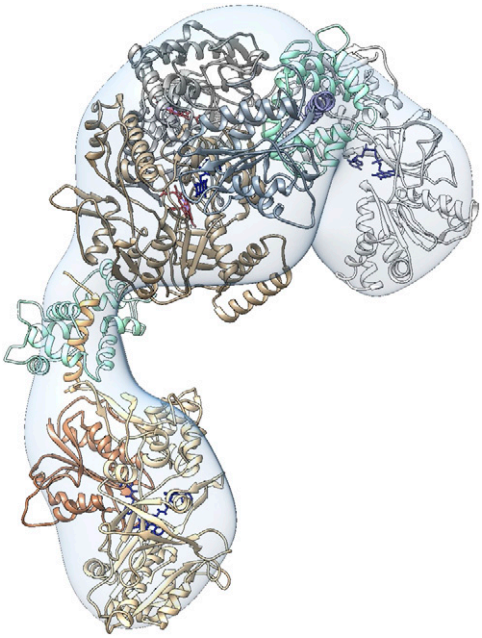

Movie S3. A 360° rotation of a group III (output state) EM structure fit with crystal structures and homology models.

Movie S3